Restructured mitochondrial-nuclear interaction in *P. falciparum* dormancy and persister survival of artemisinin exposure

Sean V. Connelly[1], Javier Manzella-Lapeira[2], Zoë C. Levine[1], Joseph Brzostowski[2], Ludmila Krymskaya[2], Rifat S. Rahman[1], Juliana M. Sá[1], Thomas E. Wellems[1*]

[1] Laboratory of Malaria and Vector Research (LMVR), National Institute of Allergy and Infectious Diseases (NIAID), National Institutes of Health (NIH), Bethesda, MD

[2]Laboratory of Immunogenetics (LIG), National Institute of Allergy and Infectious Diseases (NIAID), National Institutes of Health (NIH), Bethesda, MD

*Corresponding author

TEW: twellems@niaid.nih.gov

ABSTRACT

Artemisinin and its semi-synthetic derivatives (ART) are fast acting, potent antimalarials; however, their use in malaria treatment is frequently confounded by recrudescences from bloodstream *Plasmodium* parasites that enter into and later reactivate from a dormant persister state. Here we show that the mitochondria of dihydroartemisinin (DHA)-exposed persisters are dramatically altered and enlarged relative to the mitochondria of young, actively replicating ring forms. Persister forms exhibit restructured mitochondrial-nuclear associations and an altered metabolic state consistent with stress from reactive oxygen species. New contacts between the mitochondria and nuclei may support communication pathways of mitochondrial retrograde signaling, resulting in transcriptional changes in the nucleus as a survival response. Further characterization of the organellar interactions and metabolic dependencies of persisters may suggest strategies to combat recrudescences of malaria after treatment.

Introduction

Artemisinin, from the Chinese natural Qinghaosu remedy, provides the basis for first line treatments of malaria worldwide, particularly for the deadliest form caused by *Plasmodium falciparum* [1]. Artemisinin and its semi-synthetic derivatives (collectively abbreviated here as ART) are among the best antimalarials for rapid clearance of parasitemia and resolution of illness [2, 3]. Yet, despite these invaluable qualities, lasting cures from ART treatment are not assured: since the time of its introduction, frequent recrudescences have been reported after ART monotherapy, necessitating the utilization of a partner drug for their prevention [4]. Various studies have identified dormant persister forms from erythrocytic-stage populations that give rise to these recrudescences [5-8]. Much remains to be understood about the nature of these persisters and how they develop from only a small fraction (estimated less than ~1% [5, 7]) of the circulating ART treated parasite population.

Although dormant hypnozoites in the liver stage cycle of certain *Plasmodium* spp. were well known, evidence was not reported until 1995 that dormant parasites could be found in erythrocytes after drug and toxin exposure. Nakazawa *et al.* [9] demonstrated the presence of a small number of the dormant parasites following destruction of the great majority of actively replicating parasites by D-sorbitol treatments or exposure to pyrimethamine. Importantly, the dormant parasites were able to survive these exposures for several days, after which the dormant parasites gave rise to recrudescent populations that were as susceptible to the

treatments as the original populations. Further, no relationship could be demonstrated between the incidence or timing of recrudescence and drug concentration to which the original population was exposed [10].

Microscopic images of dormant forms after ART exposure were presented by LaCrue *et al.* [6] and Tucker *et al.* [8]: in Giemsa-stained blood films, these forms were distinguished from actively replicating ring stages and pyknotic parasites by their small rounded appearance with magenta colored chromatin and condensed blue cytoplasm. The importance of mitochondrial membrane potential to persister viability was demonstrated by Rhodamine 123 staining and outgrowth experiments [11]. Although their metabolic pathways were found to be largely downregulated after ART exposure, dormant parasites demonstrated upregulation of some enzymes involved in fatty acid biosynthesis, pyruvate metabolism, and the isoprenoid pathway [12, 13]. Changes in the expression of cyclin and cyclin dependent kinase (CDK) genes have also been reported with dormancy and reactivation of persister forms [14].

Recent advances in methods for isolation of persister parasites, imaging of their subcellular organelles, and metabolic activity analysis offer approaches for new insights into these important *Plasmodium* stages. The application of the AiryScan principle in laser scanning microscopy provides increased resolution for organelle level imaging of individual cells, as compared to standard confocal microscopy, with improved signal-to-noise ratio from 32 detectors that collect emitted light

usually excluded [15]. Modern methods of fluorescence lifetime imaging (FLIM) with exogenous or endogenous (autofluorescent) fluorophores enable non-invasive characterization of the metabolic status of cells. In the technique of time domain autofluorescence FLIM, a laser scanning microscope (LSM) with a pulsed multiphoton laser excites the endogenous fluorophore and records the distribution of photons that are emitted over time from each pixel in an image [16, 17]. The metabolic coenzyme NADH has specific mean fluorescence lifetimes based on its free or protein bound state, allowing detection of metabolic changes and providing insight on the redox status of tissues [18]. Phasor analysis of raw FLIM data provides a 2D graphical approach that does not require fitting to a decay model, and it correlates each pixel in an image to a position in phasor space [19]. For example, metabolic characterization through the phasor approach was applied to germ cells, bacteria and primary keratinocyte cultures to assay the response of these cells to metabolic perturbations [20-22].

Here we compare the structural and metabolic phenotypes of persisters to those of actively replicating ring forms in two *P. falciparum* lines: GB4, an African clone of Ghanaian origin; and 803, a clonal line from Cambodia. These two lines differ by the *pfk13*-determined survivals of early (0–3 h post invasion) ring-stage parasites exposed to a 6 hour pulse of physiological level DHA (in ring-stage survival assays, or RSAs) [23]. Nevertheless, after exposure to these pulses of DHA, GB4 and 803 populations both develop persister parasite forms that show changes in the morphological features and volumes of mitochondria as well as

similar tight associations between the mitochondria and nuclei. In autofluorescence FLIM-phasor analysis of GB4 and 803 persisters relative to actively replicating ring forms, metabolic shifts are consistent with damage produced by DHA in the mitochondria, altered electron transport chain function, and increased free NADH and reactive oxygen species (ROS). These effects are discussed in context of what is known from findings with other biological systems and insights they may offer into the persister survival mechanism.

Results

Prolongation of the intraerythrocytic cycle occurs in *P. falciparum* lines exposed to DHA, irrespective of K13 mutation and ring survival phenotype

For the experiments of this report, four lines were chosen based on K13 genotype. Two of these lines were utilized in a genetic cross that differed in DHA ring survival phenotypes: GB4 with Kelch propeller wild type K13, and 803 with the K13 C580Y propeller polymorphism [23]. The other two lines are an isogenic pair differing at the K13 locus: 76H10 with the C580Y polymorphism, and $76H10^{C580Rev}$ with an engineered C580 wild-type (revertant) codon. Assays of ring-stage survival were performed with these four lines as previously described [24]. Zero-to-three hour ring-stage parasites were exposed for 6 hours to control vehicle (0.1% DMSO) or 700 nM DHA/0.1% DMSO treatment at t = 0 hours and percentage survivals were counted at t = 72 hours (Figure 1A). In these RSAs, K13 C580Y parasites exhibited a higher proportion of parasites that survived

DHA treatment than C580 parasites, a phenotype previously linked to C580Y inheritance [23].

Stage distributions were assessed among the survivors in the control and DHA-treated parasites of each line at *t* = 72 hours (Figure 1B). At this timepoint, all four parasite lines exhibited a higher proportion of ring-stage parasites after DHA than after control vehicle exposure, suggesting that the peak beginning of the 2nd cell cycle had been delayed until 52-56 hours after DHA treatment (Figure 1C). These findings are consistent with a previous report of ART exposure inducing a delay in the erythrocytic cycle of *P. falciparum* [25]. In another study, transcriptomic data of *P. falciparum* isolates from patients with acute malaria likewise showed evidence for decelerated ring-stage development after ART treatment [26].

A fluorescence sensor of mitochondrial potential identifies viable erythrocytic-stage GB4 and 803 parasites after DHA treatment

Peatey *et al.* [11] described the use of Rhodamine 123, a mitochondrial potential marker, with Fluorescence Activated Cell Sorting (FACS) to identify and isolate viable parasites after DHA treatment of synchronized ring stages. Among these viable parasites were two distinct populations: (1) dormant persister forms; and (2) actively growing stages that continued to progress through the cell cycle and could be removed by sequential captures in magnetic separation columns. We therefore adopted magnetic capture to enrich for persister forms after DHA

exposure. GB4 or 803 parasites at 0 – 3 hours ring-stage (post-invasion) were placed in cultures at timepoint *t* = 0 hours with control vehicle (0.1% DMSO) or 700 nM DHA/0.1% DMSO. Control or DHA-treated samples were washed twice at *t* = 6 hours and placed back into culture. At *t* = 30 hours, the DHA-treated samples were passed through a magnetically activated cell sorting (MACS) column to deplete mature-stage, hemozoin-containing parasites that had survived drug treatment, reducing but not completely removing the contribution of these stages from reinvasion into the next cycle. To isolate and compare the populations of control vehicle- and DHA-exposed GB4 and 803 parasite populations at the beginning of the 2nd erythrocytic-stage cycle, we performed FACS at *t* = 50 hours with SYBR Green I (SG) as a DNA dye and MitoTracker Deep Red FM (MT) as a mitochondrial membrane potential marker.

Representative FACS dot plots of the GB4 and 803 samples at *t* = 50 hours are shown in Figure 2. In each experiment, uninfected erythrocytes that lack SG and MT signals present in the lower left quadrant of the plot. In the upper left quadrant of the plot, the gate region labeled “PYK” counts pyknotic parasites that lack mitochondrial potential whereas, in the upper right quadrant of the plot, the gate region labeled MT+ counts parasites that exhibit mitochondrial activity. In the MT+ gate region, increasing SG and MT signals moving upward and to the right arise from the progression of young ring stages to mature stage parasites, as has been described with fluorescent markers in previous studies [27]. Clusters of ring and late stage schizonts are evident in the control populations of both

GB4 and 803. Referring to the timeline (Fig. 1C), the clusters of schizonts derive from the end of the first erythrocytic-stage cycle while the more numerous ring stages derive from the beginning of the second cycle. FACS results from the DHA-treated parasites show large numbers of pyknotic parasites that lack mitochondrial potential in the “PYK” region, as expected from drug killing. Surviving parasites, however, are evident in both the GB4 and 803 populations, with greater counts of 803, consistent with their higher RSA survival levels compared to GB4 parasites (Fig. 1A). Thus, in the DHA-treated 803 MT+ distribution, the presence of trophozoites from the delay in the first intraerythrocytic cycle contributes to the appearance of a more continual representation of developmental stages across the intensity spectrum.

While the SG+MT+ subsets of the GB4 and 803 control populations contained predominantly ring-stage forms, the DHA-treated parasites after passage through the magnetic column at *t* = 30 hrs were enriched for persister forms [11].Thus, FACS at *t* = 50 hours identified a distribution of persisters as well as rings and mature stages that escaped removal by the single magnetic column. From this distribution, we were able to use the criteria of size and fluorescence intensity to identify and individually study these different forms.

AiryScan Imaging Reveals Organelle Level Changes in GB4 and 803 Persisters

Isolated persister and ring-stage forms were imaged by high-resolution AiryScan Microscopy (ASM) and compared for fluorescent mitochondrial and nuclear volumes, the shapes of these volumes as indicators of organellar morphology, and the mean distances between these volumes as indicators of relative mito-nuclear positioning.

Figure 3 shows representative surface renderings of the volumes of nuclear DNA and mitochondrial fluorescence regions in three separate experiments with control or DHA-treated GB4 and 803 parasites. Examples of distance determinations between the centers of volume are shown in Figure 3 – Figure Supplement 1. In the control GB4 and 803 samples, the nuclear DNA (green) and mitochondrial (red) volumes of the ring forms were clearly separated from one another. Nuclear DNA volumes presented with an oblate or boxy appearance and were larger in volume than the mitochondria. The mitochondrial volumes exhibited an oblate appearance, consistent with a recent account of localized mitochondrial regions in ring-stage parasites [28]. Long tubular structures [29] were not characteristic of the MT-stained mitochondria in this study.

After DHA treatment of the synchronized GB4 parasites followed by magnetic column separation at t = 30 hrs, actively growing parasites were mostly eliminated, and surviving persisters greatly predominated in the DHA-treated GB4 population captured for analysis at t = 50 hours. Figure 3A (right panel)

presents the nuclear and mitochondrial morphologies of six parasites from this population: one exhibited a smooth oblate mitochondrion separate from the nucleus as is characteristic of an actively growing ring-stage form, whereas the five others had distinctly different appearances, with rumpled and corrugated mitochondria in close approximation to the nuclei. The mitochondria partially enwrapped the nuclei and were often enlarged compared to the control ring-stage parasites. Contact sites appeared to be present between the nuclear DNA and mitochondria as another potential feature of the persister phenotype.

Because single column separation at *t* = 30 hrs did not completely remove actively replicating parasites from the DHA-treated 803 parasites (Figure 2, bottom right panel; three daily column separations would have been required for more complete isolation of persisters [7]), the parasites imaged by ASM at *t* = 50 hours comprised a mixed population of persister and ring-stage forms. In comparison to the DHA-treated GB4 population, images from the DHA-treated 803 population showed more frequent examples of cells with smooth surfaced mitochondria separate from the nuclei, similar to those of the control 803 population (Figure 3B, right panel). Other images of DHA-treated 803 parasites showed rumpled, corrugated mitochondria in close approximation to nuclei as observed for the DHA-treated GB4 persisters (Figure 3B, right panel). These findings confirmed the presence at *t* = 50 hours of a mixed population of persisters and actively replicating ring stages in the DHA-treated 803 sample, consistent with the results shown in Figure 2.

Population measures of mito-nuclear distance and organelle volumes in persisters and actively replicating parasites

To quantify the phenotypes of persisters *vs.* actively replicating ring-stage parasites, mito-nuclear distances, mitochondrial volumes, and nuclear volumes were determined from parasites of the control vehicle- and DHA-treated GB4 and 803 populations. For GB4 parasites (Figure 4A, left), a mito-nuclear median distance and interquartile range (IQR) of 0.56 (0.32 – 0.98) µm was obtained from the control, untreated population of ring-stages (n = 167), whereas a much smaller median distance of 0.19 (0.11 – 0.28) µm was obtained from the population of DHA-treated GB4 parasites that predominantly consisted of persisters (n = 167) ($p < 0.0001$, unpaired t-test). For 803 parasites (Figure 4B, left), the control vehicle-treated population of ring-stages presented a mito-nuclear median distance and interquartile range (IQR) of 0.39 (0.25 – 0.53) µm (n = 190), while the median distance of 0.31 (0.17 – 0.49) µm (n = 158) in DHA-treated 803 parasites was not significantly smaller ($p = 0.50$, unpaired t-test). The insignificance of this difference between the control and DHA-treated 803 populations is consistent with presence of mixed persisters and surviving active ring-stage forms in the DHA-treated 803 population.

Mitochondrial volume comparisons of control and DHA-exposed GB4 or 803 parasites revealed an increase in the mitochondrial volume after DHA treatment. In control GB4 parasites (Figure 4A, right), the median mitochondrial volume and

IQR was 0.26 (0.20 – 0.34) μm^3, which was much smaller than the post DHA treatment mitochondrial median volume of 1.30 (0.64 – 1.9) μm^3, representing a 5-fold increase ($p < 0.0001$, unpaired t-test). In control 803 parasites, the median mitochondrial volume was 0.31 (0.20 – 0.43) μm^3 while the DHA-exposed median volume was 0.54 (0.23 – 1.5) μm^3 (Figure 4B, right) ($p < 0.0001$, unpaired t-test). Compared to the results from GB4 parasites, the less dramatic increase of median mitochondrial volume in DHA-exposed 803 parasites at $t = 50$ hours may be explained by its mixed population of persisters, with large mitochondrial volumes, plus actively replicating ring forms, with smaller mitochondrial volumes. These findings with GB4 and 803 parasites are consistent with the increased mitochondrial volumes that have been reported from other studies of ART-treated *Plasmodium* and *Toxoplasma gondii* [30, 31].

For GB4 parasites, the median nuclear DNA volume in the control population was 1.1 (0.85 – 1.4) μm^3, whereas DHA-exposed parasites presented a smaller median volume of 0.83 (0.57 – 1.1) μm^3 (Figure 4 – Figure Supplement 1) ($p = 0.0012$, unpaired t-test). In control 803 parasites, the median nuclear DNA volume was 1.8 (1.2 – 2.2) μm^3 and in DHA-treated 803, a slightly larger median nuclear DNA volume was observed, 2.1 (1.5 – 2.8) μm^3 (Figure 4 – Figure Supplement 1) ($p < 0.0001$, unpaired t-test).

Isolation and Characterization of Persister Parasites 5 and 11 Days after DHA Treatment

After examining the morphological characteristics of persister mitochondria and quantifying their close apposition to nuclei at *t* = 50 hours, we looked for the presence of these features in persisters 1 – 2 weeks old, before their recrudescence in culture. Accordingly, we followed the *in vitro* cultures of synchronized 803 and GB4 parasites after treatment with 700 nM DHA for 6 hours and three successive 5% D-Sorbitol treatments at 24, 48 and 72 hours, as described previously [32]. Figure 4C presents the resulting dormancy and recrudescence time courses, beginning from parasitemias of 2% upon DHA exposure, through the dormancy period, to recrudescence of the 803 and GB4 parasitemias 16 and 20 days later. Samples of the GB4 and 803 persister populations were sorted, and MT-positive subsets were collected at day 5 and day 11 for imaging and analysis.

Representative ASM volume images of GB4 and 803 parasites are shown in Figure 4D for day 5 and Figure 4E for day 11. On day 5, persister morphology was observed in the 803 line, as evidenced by the large and rumpled mitochondrial volumes enwrapping the nucleus (Figure 4D). On day 11, this persister morphology continued to characterize the GB4 and 803 parasites and was similar to the morphology observed earlier, at *t* = 50 hours and at 5 days. However, 803 parasites of the day 11 population were also found with smaller oblate mitochondria separate from the nucleus, *i.e.* with features that resembled the actively growing ring-stage forms of the original 803 control group (Figure 4E, compared with Figure 3B). Such evidence for actively growing ring-stage forms

among persisters in the 11-day 803 population is consistent with waking from dormancy at the beginning of the recrudescence curve shown in Figure 4C.

In support of the presence of active ring stages wakened from 803 persisters, the median mito-nuclear distance of the 803 population at 11 days (0.24 (0.15 – 0.39) µm) was greater than that of the GB4 population (0.20 (0.13 – 0.28) µm) ($p = 0.0187$, unpaired t-test) (Figure 4B, left and Figure 4A, left). Before the waking events, ASM of the 803 parasites was performed on day 5 after DHA treatment and the small median distance typical of a pure persisters population was observed (0.18 (0.087 – 0.26) µm) (Figure 4B). On day 11, the median mitochondrial volume of GB4 persisters (2.1 (1.6 – 2.7) μm^3) was larger than that of 803 parasites (0.71 (0.24 – 1.6) μm^3) ($p < 0.0001$, unpaired t-test) (Figure 4A, right and Figure 4B, right). Consistent with the persister phenotype, a larger median mitochondrial volume of 1.5 (1.2 – 1.8) μm^3 was observed in the 803 persister parasites on day 5 *vs.* day 11 (Figure 4B, right) ($p < 0.0001$, unpaired t-test). In terms of nuclear volume on day 11 (Figure 4 – Figure Supplement 1), the GB4 persister median fluorescence volume of 1.5 (1.1 – 1.9) μm^3 was insignificantly different from the median volume of persister 803 parasites (1.6 (1.2 – 2.2) μm^3; $p = 0.09$), unpaired t-test). However, on day 5, persister 803 parasites had a smaller nuclear volume of 1.2 (1.1 – 1.5) μm^3 than on day 11 ($p < 0.0001$, unpaired t-test).

Metabolic Phenotyping of GB4 and 803 Parasites at *t* = 50 Hours

FLIM as a metabolic imaging technique detects the state of native fluorophores, particularly nicotinamide adenine dinucleotide (NADH). NADH, a metabolic coenzyme can be used as an autofluorescence indicator of the redox state of cells [33], because this molecule has characteristic emission spectrum in its enzyme bound vs. free state [34]. These two states have characteristic fluorescence lifetimes in FLIM, with enzyme bound NADH having a longer fluorescence lifetime and free NADH having a shorter fluorescence lifetime [18]. To study parasites for autofluorescence FLIM, control and DHA-treated GB4 or 803 parasites were stained only with MT to avoid spectral overlap with the broad SG spectrum [35], and MT fluorescence-positive parasites were sorted by FACS, allowed to adhere to a poly-lysine-coated PDMS microwell, and imaged in the DIC and MT emission channels of the confocal microscope (Figure 5A). At least ten million photon events were counted while limiting the time of exposure of these parasites to 750 nm excitation. Comparison of intensity images in the same field of view before and after FLIM acquisition confirmed little or no photobleaching. To process each field of view, a masking strategy was used to isolate the photon distributions for only ring-stage or persister forms, and the FLIM data from each pixel were collected in the region of interest.

Phasor analysis of the raw autofluorescence FLIM data [20] was utilized to assess the ratio of bound vs. free NADH in a cell or organism (Figure 5A). Figure 5B presents FLIM-phasor comparisons of actively replicating control *vs.* DHA-treated populations of GB4 and 803 parasites at t = 50 hours. In three

separate comparisons performed on different days, the phasor space distributions of the data from the individual parasites were plotted, and asterisks were used to mark the mean phasor positions of the control and DHA-treated parasite distributions. In the GB4 comparisons (Figure 5B, left panel), the phasor distribution of the DHA-treated population was shifted to the right of the untreated actively growing control ring stages, indicative of a relatively greater level of free NADH and diminished metabolic state of the persister phenotype (control: (0.75, 0.22), DHA: (0.80, 0.19); $p < 0.0001$, Pillai trace). In the 803 results (Figure 5B, right panel), the DHA-treated population had only a higher S coordinate than the control group (control: (0.63, 0.14), DHA: (0.63, 0.16); $p < 0.05$, Pillai trace). Little or no shift to the right in the phasor position of the DHA-treated 803 population was consistent with the presence of metabolically active ring forms along with dormant persisters in this population at t = 50 hours.

Metabolic Phenotypes of GB4 and 803 Persisters Prior to Recrudescence *in vitro*

Autofluorescence FLIM and phasor analysis were used to also examine the metabolic states of the DHA/sorbitol treated GB4 and 803 parasites on day 5 (Figure 5C, left panel) and day 11 of dormancy (Figure 5C, right panel). On these days, the mean coordinates of the GB4 and 803 distributions were located on the right side of the phasor plot. Although the coordinates of the mean phasor positions from each assessment may be affected by particulars of the culture conditions and experimental manipulations, we note the large shift of the mean

803 signal from its position at *t* = 50 hours, consistent with the higher level of free NADH in the purer population of persisters (DHA *t* = 50 hours coordinates (0.63, 0.16) *vs.* DHA day 5 coordinates (0.77, 0.21); $p < 0.0001$, Pillai Trace; compare Figures 5B, right panel and 5C, left panel). In the 803 line, the calculated mean position of the distribution at day 11 trended to the left of the position at day 5 (DHA day 5 coordinates (0.77, 0.21) *vs.* DHA day 11 coordinates (0.74, 0.22); $p = 0.05$, Pillai Trace; compare Figure 5C, right panel and 5C, left panel). This trend suggests that a relatively greater level of bound NADH was developing on day 11, consistent with the aforementioned presence of active ring forms recrudescing from the 803 persister population.

Discussion

Subsequent to early proposals that dormant erythrocytic stages are responsible for recrudescences of *P. falciparum* infection after treatment with artemisinin drugs [5], *in vitro* as well as *in vivo* studies continued to build evidence for the importance of these parasite forms in failures of the artemisinins to achieve complete cure [6-8, 23, 32, 36, 37]. Dormant parasites were found to be small and to have characteristic features that distinguish them from pyknotic or ring-stage forms in erythrocytes: in Giemsa-stained thin blood smears, these features include a magenta nucleus bordered by a small region of blue cytoplasm [8, 32, 37]. Mitochondrial activity is vital to the survival of dormant forms and their return to active propagation; this activity has enabled the identification and separation of these forms by fluorescent markers specific for mitochondrial membrane

potential [11]. In the present study, we have used FACS sorting, ASM, and autofluorescence FLIM-phasor analysis to characterize signature changes in the mitochondria of persisters that develop after exposure of *P. falciparum*-infected erythrocytes to DHA.

Remarkable morphological differences distinguish the mitochondria of DHA-induced persisters from the mitochondria of actively growing ring-stage parasites. The mitochondria of persisters have a more rumpled and corrugated appearance that appears within 50 hours of DHA exposure, whereas smooth and oblate mitochondria are characteristic of the actively replicating ring-stage parasites. Along with their irregular shapes, the fluorescence volumes of persister mitochondria are often large, up to 5-fold greater than the mitochondrial volumes of ring stages. These differences are accompanied by a much reduced average separation between the mitochondria and nuclei in persisters; indeed, many ASM images suggest partial enwrapment of the nuclei by the mitochondria with contact between these organelles. Studies of the ultrastructural effects of artemisinins on various *Plasmodium* species *in vivo* have likewise found mitochondrial enlargement in electron microscopy images [30, 38-40]; among other apicomplexans, mitochondrial enlargement is reported in *Toxoplasma gondii* following artemisinin drug pressure [31].

P. falciparum persisters maintain mitochondrial enlargement in tight approximation with the nucleus throughout their period of dormancy. Open

questions remain regarding the molecular pathways underlying these changes and how they might be induced upon ART exposure. Reactive oxygen species (ROS) are induced by artemisinin in isolated *Plasmodium* and yeast mitochondria, and agents that reduce electron transport chain (ETC) activity reduce artemisinin-induced ROS production and resulting membrane damage [41]. Depolarization of mitochondrial membrane potential accompanies the disruption of mitochondrial function by artemisinin in yeast [42]. In human tumor cell lines, activation of the artemisinin endoperoxide bridge by mitochondrial heme is thought to promote generation of ROS by the electron transport chain, leading to mitochondrial dysfunction and cellular apoptosis [43]. Artemisinin-resistant lines of *Toxoplasma gondii* selected *in vitro* provided further evidence for the involvement mitochondrial pathways, as demonstrated by amplifications of mitochondrial cytochrome b and cytochrome c oxidase I genes and mutations of a DegP2 ortholog in the mitochondrial proteome [31]. Another study identified the same DegP2 ortholog in a genetic screen, genetic disruption facilitated survival of *T. gondii* exposed to lethal concentrations of DHA, and deletion of this region in *P. falciparum* resulted in higher survival in the RSA [44].

Interestingly, in breast cancer cells and mouse embryonic fibroblasts the responses to mitochondrial stress include formation of tethers between the nucleus and Nuclear Associated Mitochondria (NAM) [45]. ROS production after exposure of THP-1 derived macrophages to the fungal toxin altertoxin II was followed by relocation of mitochondria to perinuclear regions [46]. In other

systems of cancer cells, ROS may both promote and result from dysfunctional mitochondrial communications with cell nuclei and organelles including endoplasmic reticulum and peroxisomes, facilitating tumorigenesis [47]. Similarly, we speculate, ROS effects and oxidative stress may be involved in triggering the development and survival of *P. falciparum* persisters through the morphological changes of mitochondria and their repositioning to tight associations with nuclei.

Mitochondrial retrograde response (MRR) signaling provides communications from mitochondria to nuclei that promote cellular adaptations under conditions of stress [48]. In studies of MRR in breast cancer, contact microdomains between the two organelles involve cholesterol redistribution and may promote a survival response [45]. The MRR pathway is conserved among species, as exemplified by nuclear protein CLK-1 in *Caenorhabditis elegans* and its homolog in human cells COQ7, which serves as a regulator of the MRR pathway that limits ROS production [49]. In *Saccharomyces cerevisiae*, nuclear gene *Nonmitochondrial Citrate Synthase 2 (CIT2)* transcription was increased after inhibition of mitochondrial respiration [50], and mitochondrial pathways were activated in response to ER stress [51]. In these studies, mitochondria and the MRR were found to serve as barometers of cellular damage, capable of changing gene expression pathways to facilitate survival. While different mechanisms of endoperoxide activation and target impairment by carbon-centered or oxygen-centered radicals have been proposed in the damage of malaria parasites by ART, rapidly killing is thought to result from depolarization of the parasite

mitochondrial and plasma membranes upon exposure to ROS, initiated by iron bioactivation of ART or by iron-dependent oxidative stress [52]. In the present work, changes in mitochondrial morphology, reduced mito-nuclear distances, and metabolic consequences induced by DHA exposure may be tied to gene expression responses involved in persister formation as a survival mechanism. These responses may relate to an innate growth bistability phenomenon whereby a fraction of the drug-exposed population switches into the metabolic quiescence of persister forms, as we have discussed elsewhere [53].

Our findings from autofluorescence FLIM-phasor analysis indicate an increased ratio amount of free NADH in persisters relative to actively replicating ring-stage parasites. This measure relates to the redox state of the cells. In other systems, human breast cell lines exposed to potassium cyanide (KCN) treatment or exposed to hypoxic conditions, autofluorescence FLIM revealed a higher amount of free NADH due to inhibition of cellular respiration [54]. Increased concentrations of free NADH in the mitochondria have been shown to promote increased ROS production [55]. When assaying ART activity in tumor cell lines, ETC function in the mitochondria was found to be essential for apoptosis through ROS production [43]. Taken together, these findings suggest that activation of the endoperoxide bridge of artemisinin by mitochondrial heme leads to altered ETC function, increased free NADH, and increased ROS species with concomitant mitochondrial damage.

After DHA treatment, a small fraction (less than ~1%; [5, 7]) of the parasite population survives killing by entering the metabolically quiescent state of dormancy. In this state, persisters may avoid damage by mitochondrial signaling and modulation of essential pathways of gene expression. How is it that this small fraction of the parasite population becomes persisters while the larger fraction dies away? The answer may be a stochastic one that lies in systems of gene control. In *P. falciparum*, feedback loops could rapidly flip the growth state of some cells to dormancy, producing persister forms that can survive DHA treatment while the actively replicating parasites succumb to the toxic effects of the drug. Understanding these feedback loops and the metabolic and functional features of persisters may lead to new chemotherapeutic approaches that can prevent clinical recrudescences.

Materials and Methods

Parasite Cultivation

Human erythrocytes were obtained weekly from Virginia Blood Services (Richmond, VA). Blood was washed upon arrival with filtered RPMI 1640 media (containing 25 mM HEPES and 50 µg/mL hypoxanthine) (KD Medical, Columbia, MD), and stored at 50% hematocrit in a 4˚C refrigerator for use within a week from processing. *P. falciparum* GB4 [56] and 803 [57] parasites were grown in complete culture media (cRPMI) containing 1% Albumax II (Life Technologies, CA, USA), 0.21% sodium bicarbonate (KD Medical, Columbia, MD), and 20

521 µg/mL gentamicin (KD Medical, Columbia, MD) in RPMI-1640 (KD Medical,
522 Columbia, MD), at 5% hematocrit, 37˚C, and a gas mixture containing 90% N_2,
523 5% CO_2, and 5% O_2. To monitor parasitemia, thin blood films were prepared on
524 glass slides, fixed with methanol and stained for 15 minutes with 20% Giemsa
525 staining (Sigma-Aldrich, St. Louis, MO). Using bright-field microscopy and an
526 100× oil objective, an estimated 1,000 erythrocytes were counted, and the
527 number of parasitized cells was used to estimate percentage parasitemia. In
528 recrudescence experiments, media was changed every other day and fresh
529 erythrocytes were added every four days. When media was changed, blood films
530 were made and used to monitor parasitemia.
531
532 **Ring-stage Survival Assay (RSA)**
533 803 and GB4 cultures were tightly synchronized to obtained 0 – 3 hour ring
534 stages through two successive 5% D-sorbitol treatments 46 hours apart [24].
535 Each sorbitol treatment lasted 10 minutes at room temperature. Immediately
536 following the second sorbitol treatment, cultures were adjusted to 2% parasitemia
537 and 5% hematocrit in a total volume of 10 mL in a T25 flask (Thermo Fisher
538 Scientific, Waltham, MA). Thin blood smears were prepared just before drug
539 exposure. Cultures were then treated at a final concentration of 0.1% DMSO or
540 700 nM DHA/0.1% DMSO by addition of 10 µl of DMSO or 10 µl of 700 µM DHA
541 for 6 hours. After 6 hours of incubation, cells were washed and returned to
542 culture in drug-free cRPMI. Sixty-six to ninety hours post DHA treatment, thin
543 blood smears were prepared, fixed with 100% methanol, and stained with 20%

Giemsa (Sigma-Aldrich, St. Louis, MO). Slides identifications were blinded from the investigators while parasitemia counts were obtained.

Dihydroartemisinin Treatment and Magnetic Removal of Mature Stages

803 and GB4 parasites were synchronized and treated with the control vehicle or DHA as above. Thirty hours after the initiation of treatment, the DHA treated culture was passed over a magnetically-activated cell sorting LD column (Miltenyi Biotec, Auburn, CA) to deplete the culture of parasites that escaped the DHA treatment and progressed past ring-stage. The same methodology as Teuscher *et al.* [7] was applied to the use of the LD column. Pelleted cells from culture were suspended in 2 mL of cold cRPMI and passed three times through the column over a period of 3 – 5 hours. Afterwards, the column was washed with 30 mL of cRPMI. Eluates were combined and pelleted at 2,500 rpm for 5 minutes, resuspended in 10 mL of cRPMI, and returned to culture. As the parasitized erythrocytes approached maturity, the cultures were placed on a rotator in the 37˚C incubator to minimize the occurrence of multiply-infected relative to singly-infected cells.

Dihydroartemisinin Recrudescence Assay

Tightly synchronized 803 and GB4 parasites, at approximately 2% ring-stage parasitemia, were treated with 700 nM of DHA for 6 hours. At 24, 48 and 72 hours post DHA treatment, the cells of both cultures were treated with 10 mL of

5% D-Sorbitol for 30 minutes at 37˚C and washed twice with cRPMI. This treatment removed mature stage parasites that survived the DHA treatment. Parasitemia was monitored by microscopy while media was changed on alternate days and fresh erythrocytes were added every four days until recrudescence.

Fluorescence Associated Cell Sorting (FACS)

At *t* = 50 hours, cells from 1 mL of each culture were pelleted and washed three times with 1ml of 1× HBSS (Gibco, Waltham, MA) containing 2% fetal bovine serum (FBS; Gibco, Waltham, MA). Washed samples were stained with 0.4× SG (Invitrogen, Waltham, MA) for DNA content and 0.1 µM MT (Invitrogen, Waltham, MA) for mitochondrial potential [58]. Samples for FLIM analysis were stained only with 0.1 µM MT to avoid SG spectral overlap (bleedthrough) with the endogenous FLIM signal [35]. Control 0.1% DMSO vehicle-treated and DHA-treated samples were filtered through a 35 µm filter (Corning, Corning, NY) immediately before sorting.

Cells were sorted by using the BD FACS Aria Fusion, and gating was performed using the BD FACSDiva™ software (BD Biosciences, Franklin Lakes, NJ). For ASM, samples underwent two sorting steps: 1) isolation of infected from uninfected erythrocytes and 2) separation of parasite populations by DNA and mitochondrial signals. The first step enriched infected cells by collecting 1 million SG positive cells. Enrichment removes the vast majority of uninfected erythrocyte

allowing for more accurate sorting of live and dead parasites in the second step. A highly pure sorting modality (4-way purity sorting for FACS Aria Fusion) was chosen for the second round of sorting. Enriched samples were collected in polystyrene round-bottom 5 mL tubes (Corning, Corning, NY) with 1 mL of 1× HBSS containing 2% FBS, pelleted at 2500 rpm for 5 minutes in the 5 mL polystyrene tube, resuspended, and sorted into two populations for each sample (Figure 2). Parasites in the left gate were used for a Giemsa-stained thin blood smear while parasites in the right gate were used for ASM. All four samples were collected in polystyrene round-bottom 5 mL tubes (Corning, Corning, NY) with 1 mL of 1× HBSS/2% FBS.

For autofluorescence FLIM, samples underwent a single step sorting. The MT positive cells were collected in polystyrene round-bottom 5 mL tubes (Corning, Corning, NY,) with 1 mL of 1× HBSS/2% FBS.

Data analyses were conducted using FCS Express (De Novo Software, Pasadena, CA).

AiryScan Microscopy Analysis

A 10 µm x 10 µm polydimethylsiloxane (PDMS) stencil microwell (Alvéole, Paris, France) was placed inside each well of a Lab-Tek 8 well chamber (Thermo Fisher Scientific, Waltham, MA). Ten µl of 0.01% poly-lysine (Sigma-Aldrich, St. Louis, MO) was added to the microwell and incubated for 30 minutes at room

temperature to allow poly-lysine to adhere to the slide. Afterwards, the microwell was washed twice with 10 µL of 1× HBSS to remove unbound poly-lysine. The DMSO and DHA-treated parasites positive for SG/MT were transferred to 1.5 mL tubes, spun down at 2,500 rpm for 3 minutes and resuspended in 20 µL of remaining wash buffer. Ten µL of cell suspension was added directly to the center of the poly-lysine coated microwell and incubated for 30 minutes at room temperature in the dark. Lastly, 200 µL of a 1:4 dilution of Intracellular (IC) Fixation Buffer (Invitrogen, Waltham, MA) in cell culture water (Gibco, Waltham, MA) was added to the chamber. The chamber was covered with a plastic membrane and stored at 4˚C for imaging within the following 24 hours. Parasites were imaged using the Zeiss LSM 880 with AiryScan. Afterwards, the AiryScan processed images were analyzed using Imaris 9.1.2 and volumes were adjusted. In the majority of cells, the small and low level mitochondrial DNA SG fluorescence was clearly distinct and excluded in the analysis. In a few cells, mitochondrial DNA fluorescence was not visible or was merged during thresholding of the DNA volume. Mitochondrial DNA regions were excluded if possible. The volumes of the mitochondrial and DNA volume were calculated as well as the distance between these volumes.

Autofluorescence FLIM and Phasor Analysis

When NADH undergoes multi-photon excitation, photons are released over time as NADH returns to its ground state, establishing a pattern of fluorescence decay that can be detected over a period of nanoseconds. The lifetime of decay differs

for NADH in its free (0.4 nanoseconds) or protein bound state (1 nanosecond), which allows for the quantification of the redox state of the organism or tissue under study [18]. In an early example of use of this observation, Chance *et al.* [34] demonstrated increases of the characteristic emission spectrum from NADH in rat organs under anoxic conditions; further, this spectrum matched the NADH emission spectrum from isolated mitochondria. With recent technical and computation advances, fluorescence emission data can translated into phasor space, a fit-free method that allows for the direct transform of each pixel of an image with a fluorescence decay to its corresponding phasor position [19]. Each fluorescence decay from each pixel undergoes a Fourier transform and is represented as a vector object with two Cartesian coordinates, one coordinate as the real part of the Fourier transform (G) and while the other as the imaginary part (S) [59]. The phasor plane is bounded by a “universal semicircle” that ranges from 0 to 1.0 on the G axis (cosine transform) and 0 to 0.5 on the S axis (sine transform). Single exponential decays fall along the boundary of the universal semicircle while multi-exponential decays fall within the semicircle, where they are subject to the law of phasor addition [60]. Autofluorescence FLIM of endogenous fluorophores, such as free and protein bound NADH, typically yields curves of multi-exponential decay and phasor coordinates within the universal semicircle. Greater relative amounts of free NADH shift the vector positions to the right side of the graph (shorter lifetimes) whereas greater amounts of protein-bound NADH shift the vector positions to the left (longer lifetimes) [61]. Through

the phasor-FLIM approach, the effects of different treatments on metabolism can be conveniently visualized by shifts of the vector position on the phasor plot [62].

DHA-treated or control parasites stained with MT were seeded onto a microwell in an 8-well chamber coated with 0.01% poly-lysine. A confocal image was acquired using a Zeiss LSM 780 for each field of view with two channels: Differential Interference Contrast (DIC) and MT emission (633nm excitation and emission collected 640 – 740 nm range). Next, emission data were collected from the given field of view with the integrated Coherent Chameleon II Ti:Sapphire femtosecond-pulsed laser tuned to 750 nm. Photons for lifetime data fitting were collected using a Becker & Hickl TCSPC DCC-100 control card with two HCM-130 GaAsP hybrid detectors. A 525 nm dichroic separated the emission into the detectors and a 480/40 bandpass filter was used with the short wavelength detector. Each field of view was scanned until at least ten million photon events were collected. Phasor values were calculated for each pixel with the SPCImage software. The resulting files were exported, and a custom MATLAB algorithm used the signal from the MT confocal images to threshold the mitochondria, obtain the mean phasor values, and run statistical tests.

Outgrowth Using Sorted Parasitized Cells

Outgrowth experiments were used to investigate parasite viability after FACS. For this purpose, control and DHA-treated samples at t = 50 hours were obtained

through three gates: SG/MT Dim (SG/MT^D), SG/MT Intermediate (SG/MT^I) and SG/MT Bright (SG/MT^B) (Supplementary File 1). Each population was placed into a polystyrene tube with 1× HBSS/2% FBS at a final concentration of 1 mL. One hundred µL was taken from these samples for a blood film, and the cells in the samples were pelleted at 2,500 rpm for 5 minutes, resuspended in 180 µL of cRPMI, and transferred to a 96 well plate. Twenty µL of a 50% erythrocyte stock were added to each well to obtain a 5% hematocrit culture. Media were changed on alternate days and 150 µL of 3.3% hematocrit solution were added every 4 or 5 days to replenish erythrocytes lost to sampling. The parasitemia in each well was monitored through thick and thin smears, using 1 µL of parasitized erythrocytes for each smear, and the time it took for the parasitemia to reach 0.5% was recorded.

Parasite viability was also verified for both control or DHA-treated GB4 and 803 parasites, utilizing the SG and MT stained samples (Supplementary Files 1 and 2).

Statistical Analysis

AiryScan datasets were compared by unpaired t-tests calculated with Graphpad Prism version 8.4.3. Autofluorescence FLIM-phasor datasets were compared through Pillai trace calculations in MATLAB version 2019b. Summarized statistics are shown in Supplementary File 3.

Acknowledgements

We thank Tom Moyer, Teresa Hawley, and David Stephany in the Flow Cytometry Section of the Research Technologies Branch for their advice on FACS sorting, and Susan Pierce for supporting experiments at the Laboratory of Immunogenetics, NIAID. This work was funded by the NIAID Division of Intramural Research.

Competing interests

No competing interests declared.

References

1. World Health Organization (2015) Guidelines for the treatment of malaria, third edition. Geneva: World Health Organization. Report No.: 9789241549127. Available at: https://apps.who.int/iris/handle/10665/162441. Accessed 21 May 2020.
2. Dondorp A, Nosten F, Stepniewska K, Day N, & White N (2005) Artesunate versus quinine for treatment of severe falciparum malaria: a randomised trial. *Lancet* 366(9487):717-725.
3. Dondorp AM*, et al.* (2010) Artesunate versus quinine in the treatment of severe falciparum malaria in African children (AQUAMAT): an open-label, randomised trial. *Lancet* 376(9753):1647-1657.
4. Li GQ, Arnold K, Guo XB, Jian HX, & Fu LC (1984) Randomised comparative study of mefloquine, qinghaosu, and pyrimethamine-sulfadoxine in patients with falciparum malaria. *Lancet* 2(8416):1360-1361.
5. Hoshen MB, Na-Bangchang K, Stein WD, & Ginsburg H (2000) Mathematical modelling of the chemotherapy of Plasmodium falciparum malaria with artesunate: postulation of 'dormancy', a partial cytostatic effect of the drug, and its implication for treatment regimens. *Parasitology* 121 (Pt 3):237-246.
6. LaCrue AN, Scheel M, Kennedy K, Kumar N, & Kyle DE (2011) Effects of artesunate on parasite recrudescence and dormancy in the rodent malaria model Plasmodium vinckei. *PLoS One* 6(10):e26689.

7. Teuscher F*, et al.* (2010) Artemisinin-induced dormancy in Plasmodium falciparum: duration, recovery rates, and implications in treatment failure. *J Infect Dis* 202(9):1362-1368.
8. Tucker MS, Mutka T, Sparks K, Patel J, & Kyle DE (2012) Phenotypic and genotypic analysis of in vitro-selected artemisinin-resistant progeny of Plasmodium falciparum. *Antimicrob Agents Chemother* 56(1):302-314.
9. Nakazawa S, Kanbara H, & Aikawa M (1995) Plasmodium falciparum: recrudescence of parasites in culture. *Exp Parasitol* 81(4):556-563.
10. Nakazawa S, Maoka T, Uemura H, Ito Y, & Kanbara H (2002) Malaria parasites giving rise to recrudescence in vitro. *Antimicrob Agents Chemother* 46(4):958-965.
11. Peatey CL*, et al.* (2015) Mitochondrial membrane potential in a small subset of artemisinin-induced dormant Plasmodium falciparum parasites in vitro. *J Infect Dis* 212(3):426-434.
12. Chen N*, et al.* (2014) Fatty acid synthesis and pyruvate metabolism pathways remain active in dihydroartemisinin-induced dormant ring stages of Plasmodium falciparum. *Antimicrob Agents Chemother* 58(8):4773-4781.
13. Duvalsaint M & Kyle DE (2018) Phytohormones, isoprenoids, and role of the apicoplast in recovery from dihydroartemisinin-induced dormancy of Plasmodium falciparum. *Antimicrob Agents Chemother* 62(3).
14. Gray KA*, et al.* (2016) Correlation between cyclin dependent kinases and artemisinin-induced dormancy in Plasmodium falciparum in vitro. *PLoS One* 11(6):e0157906.
15. Korobchevskaya K, Lagerholm BC, Colin-York H, & Fritzsche M (2017) Exploring the potential of Airyscan microscopy for live cell imaging. *Photonics* 4(3):41.
16. Becker W*, et al.* (2004) Fluorescence lifetime imaging by time-correlated single-photon counting. *Microsc Res Tech* 63(1):58-66.
17. Berezin MY & Achilefu S (2010) Fluorescence lifetime measurements and biological imaging. *Chem Rev* 110(5):2641-2684.
18. Lakowicz JR, Szmacinski H, Nowaczyk K, & Johnson ML (1992) Fluorescence lifetime imaging of free and protein-bound NADH. *Proc Natl Acad Sci U S A* 89(4):1271-1275.
19. Digman MA, Caiolfa VR, Zamai M, & Gratton E (2008) The phasor approach to fluorescence lifetime imaging analysis. *Biophys J* 94(2):L14-16.
20. Stringari C*, et al.* (2011) Phasor approach to fluorescence lifetime microscopy distinguishes different metabolic states of germ cells in a live tissue. *Proc Natl Acad Sci U S A* 108(33):13582-13587.
21. Bhattacharjee A, Datta R, Gratton E, & Hochbaum AI (2017) Metabolic fingerprinting of bacteria by fluorescence lifetime imaging microscopy. *Sci Rep* 7(1):3743.
22. Pouli D*, et al.* (2016) Imaging mitochondrial dynamics in human skin reveals depth-dependent hypoxia and malignant potential for diagnosis. *Sci Transl Med* 8(367):367ra169.

23. Sá JM, *et al.* (2018) Artemisinin resistance phenotypes and K13 inheritance in a Plasmodium falciparum cross and Aotus model. *Proc Natl Acad Sci U S A* 115(49):12513-12518.
24. Kite WA, Melendez-Muniz VA, Moraes Barros RR, Wellems TE, & Sa JM (2016) Alternative methods for the Plasmodium falciparum artemisinin ring-stage survival assay with increased simplicity and parasite stage-specificity. *Malar J* 15:94.
25. Klonis N, *et al.* (2011) Artemisinin activity against Plasmodium falciparum requires hemoglobin uptake and digestion. *Proc Natl Acad Sci U S A* 108(28):11405-11410.
26. Mok S, *et al.* (2015) Drug resistance. Population transcriptomics of human malaria parasites reveals the mechanism of artemisinin resistance. *Science* 347(6220):431-435.
27. Malleret B, *et al.* (2011) A rapid and robust tri-color flow cytometry assay for monitoring malaria parasite development. *Sci Rep* 1:118.
28. Scarpelli PH, *et al.* (2019) Melatonin activates FIS1, DYN1, and DYN2 Plasmodium falciparum related-genes for mitochondria fission: Mitoemerald-GFP as a tool to visualize mitochondria structure. *J Pineal Res* 66(2):e12484.
29. van Dooren GG, *et al.* (2005) Development of the endoplasmic reticulum, mitochondrion and apicoplast during the asexual life cycle of Plasmodium falciparum. *Mol Microbiol* 57(2):405-419.
30. Maeno Y, *et al.* (1993) Morphologic effects of artemisinin in Plasmodium falciparum. *Am J Trop Med Hyg* 49(4):485-491.
31. Rosenberg A, Luth MR, Winzeler EA, Behnke M, & Sibley LD (2019) Evolution of resistance in vitro reveals mechanisms of artemisinin activity in Toxoplasma gondii. *Proc Natl Acad Sci U S A*.
32. Breglio KF, Rahman RS, Sa JM, Roberts DJ, & Wellems TE (2018) Kelch mutations in Plasmodium falciparum protein K13 do not modulate dormancy after artemisinin exposure and sorbitol selection in vitro. *Antimicrob Agents Chemother* 62(5).
33. Chance B, Schoener B, Oshino R, Itshak F, & Nakase Y (1979) Oxidation-reduction ratio studies of mitochondria in freeze-trapped samples. NADH and flavoprotein fluorescence signals. *J Biol Chem* 254(11):4764-4771.
34. Chance B, Legallais V, & Schoener B (1962) Metabolically linked changes in fluorescence emission spectra of cortex of rat brain, kidney and adrenal gland. *Nature* 195:1073-1075.
35. Zipper H, Brunner H, Bernhagen J, & Vitzthum F (2004) Investigations on DNA intercalation and surface binding by SYBR Green I, its structure determination and methodological implications. *Nucleic Acids Res* 32(12):e103.
36. Ittarat W, *et al.* (2003) Recrudescence in artesunate-treated patients with falciparum malaria is dependent on parasite burden not on parasite factors. *Am J Trop Med Hyg* 68(2):147-152.
37. Chavchich M, Van Breda K, Rowcliffe K, Diagana TT, & Edstein MD (2016) The spiroindolone KAE609 does not induce dormant ring stages in

Plasmodium falciparum parasites. *Antimicrob Agents Chemother* 60(9):5167-5174.

38. Ellis DS*, et al.* (1985) The chemotherapy of rodent malaria, XXXIX. Ultrastructural changes following treatment with artemisinine of Plasmodium berghei infection in mice, with observations of the localization of [3H]-dihydroartemisinine in P. falciparum in vitro. *Ann Trop Med Parasitol* 79(4):367-374.

39. Kawai S, Kano S, & Suzuki M (1993) Morphologic effects of artemether on Plasmodium falciparum in Aotus trivirgatus. *Am J Trop Med Hyg* 49(6):812-818.

40. Jiang JB, Jacobs G, Liang DS, & Aikawa M (1985) Qinghaosu-induced changes in the morphology of Plasmodium inui. *Am J Trop Med Hyg* 34(3):424-428.

41. Wang J*, et al.* (2010) Artemisinin directly targets malarial mitochondria through its specific mitochondrial activation. *PLoS One* 5(3):e9582.

42. Li W*, et al.* (2005) Yeast model uncovers dual roles of mitochondria in action of artemisinin. *PLoS Genet* 1(3):e36.

43. Mercer AE, Copple IM, Maggs JL, O'Neill PM, & Park BK (2011) The role of heme and the mitochondrion in the chemical and molecular mechanisms of mammalian cell death induced by the artemisinin antimalarials. *J Biol Chem* 286(2):987-996.

44. Harding CR*, et al.* (2020) Genetic screens reveal a central role for heme metabolism in artemisinin susceptibility. *Nat Commun* 11(1):4813.

45. Desai R*, et al.* (2020) Mitochondria form contact sites with the nucleus to couple pro-survival retrograde response. *bioRxiv*:445411.

46. Del Favero G, Hohenbichler J, Mayer RM, Rychlik M, & Marko D (2020) Mycotoxin altertoxin II induces lipid peroxidation connecting mitochondrial stress response to NF-kappaB inhibition in THP-1 macrophages. *Chem Res Toxicol* 33(2):492-504.

47. Xia M*, et al.* (2019) Communication between mitochondria and other organelles: a brand-new perspective on mitochondria in cancer. *Cell Biosci* 9:27.

48. Butow RA & Avadhani NG (2004) Mitochondrial signaling: the retrograde response. *Mol Cell* 14(1):1-15.

49. Monaghan RM*, et al.* (2015) A nuclear role for the respiratory enzyme CLK-1 in regulating mitochondrial stress responses and longevity. *Nat Cell Biol* 17(6):782-792.

50. Liao XS, Small WC, Srere PA, & Butow RA (1991) Intramitochondrial functions regulate nonmitochondrial citrate synthase (CIT2) expression in Saccharomyces cerevisiae. *Mol Cell Biol* 11(1):38-46.

51. Hijazi I, Knupp J, & Chang A (2020) Retrograde signaling mediates an adaptive survival response to endoplasmic reticulum stress in Saccharomyces cerevisiae. *J Cell Sci* 133(6).

52. Antoine T*, et al.* (2014) Rapid kill of malaria parasites by artemisinin and semi-synthetic endoperoxides involves ROS-dependent depolarization of the membrane potential. *J Antimicrob Chemother* 69(4):1005-1016.

53. Wellems TE, Sa JM, Su XZ, Connelly SV, & Ellis AC (2020) 'Artemisinin Resistance': Something new or old? Something of a misnomer? *Trends Parasitol*.
54. Bird DK*, et al.* (2005) Metabolic mapping of MCF10A human breast cells via multiphoton fluorescence lifetime imaging of the coenzyme NADH. *Cancer Res* 65(19):8766-8773.
55. Murphy MP (2009) How mitochondria produce reactive oxygen species. *Biochem J* 417(1):1-13.
56. Hayton K*, et al.* (2008) Erythrocyte binding protein PfRH5 polymorphisms determine species-specific pathways of Plasmodium falciparum invasion. *Cell Host Microbe* 4(1):40-51.
57. Amaratunga C*, et al.* (2012) Artemisinin-resistant Plasmodium falciparum in Pursat province, western Cambodia: a parasite clearance rate study. *Lancet Infect Dis* 12(11):851-858.
58. Amaratunga C, Neal AT, & Fairhurst RM (2014) Flow cytometry-based analysis of artemisinin-resistant Plasmodium falciparum in the ring-stage survival assay. *Antimicrob Agents Chemother* 58(8):4938-4940.
59. Dalbey RE, Weiel J, Perkins WJ, & Yount RG (1984) Resolution of multiple fluorescence lifetimes in heterogeneous systems by phase-modulation fluorometry. *J Biochem Biophys Methods* 9(3):251-266.
60. Jameson DM, Gratton E, & Hall RD (1984) The measurement and analysis of heterogeneous emissions by multifrequency phase and modulation fluorometry. *Applied spectroscopy reviews* 20(1):55-106.
61. Ranjit S, Malacrida L, Jameson DM, & Gratton E (2018) Fit-free analysis of fluorescence lifetime imaging data using the phasor approach. *Nat Protoc* 13(9):1979-2004.
62. Aguilar-Arnal L*, et al.* (2016) Spatial dynamics of SIRT1 and the subnuclear distribution of NADH species. *Proc Natl Acad Sci U S A* 113(45):12715-12720.

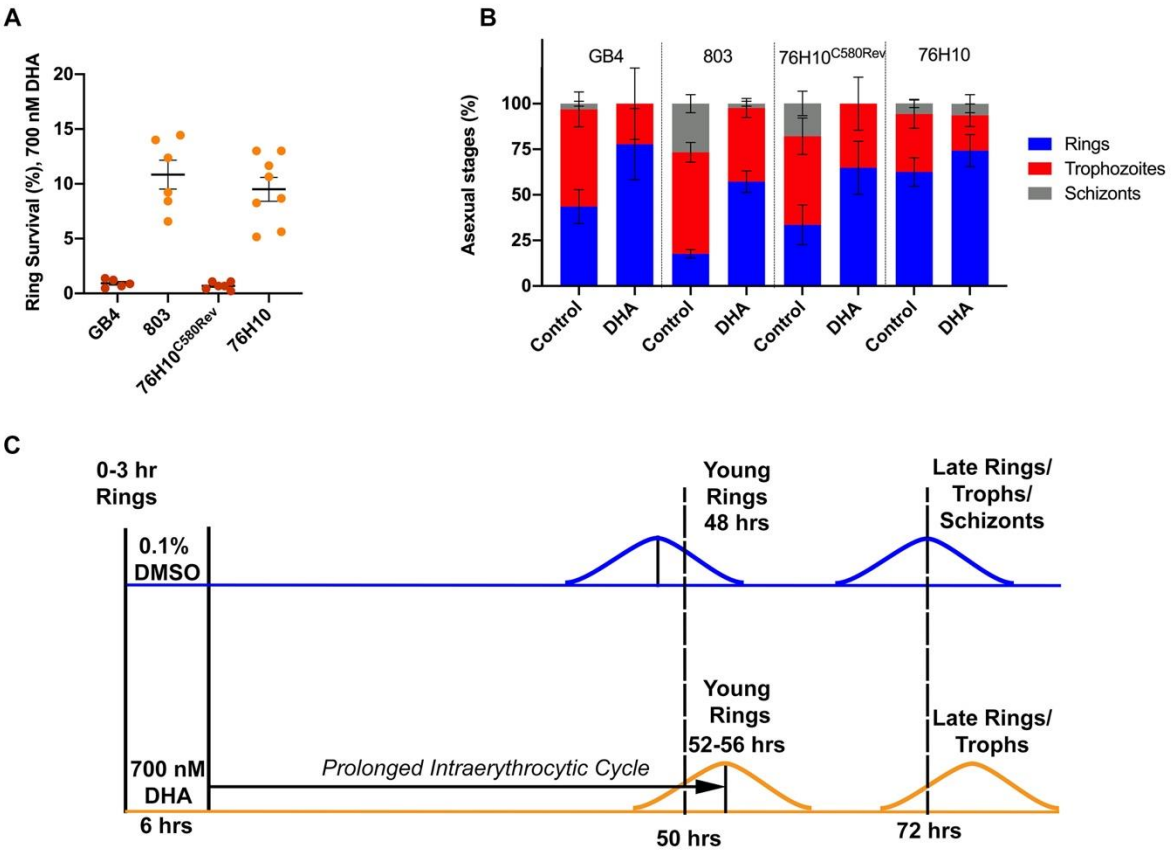

Figure 1. Intraerythrocytic cycle delay exhibited by DHA-treated *P. falciparum* parasites *t* = 72 hours after DHA incubation. GB4, 803, 76H10^{C580Rev} and 76H10 parasite lines underwent a standard Ring-stage Survival Assay (RSA) procedure, in which cultures at approximately 2% parasitemia were treated with control 0.1% DMSO (vehicle) or 700 nM DHA at *t* = 0 hours. After 6 hours of incubation, the samples were washed and returned to culture. At *t* = 72 hours, the stage distributions were counted and percentage survivals were calculated. (**A**) Ring-stage Survivals. At the *t* = 72 hour timepoint, the percent survival was calculated for each strain through dividing the number of surviving DHA-treated parasites by the number of control vehicle-treated parasites. After DHA treatment, GB4 and 76H10^{C580Rev} parasites (C580 K13 propeller wild type) survived at lower levels than the C580Y propeller mutant 803 and 76H10 parasites (0.93 +/- 0.16 (mean +/- SEM, N=5) and 0.69 +/- 0.14 (mean +/- SEM, N=6) *vs.* 10.84 +/- 1.32 (mean +/- SEM, N=6) and 9.50 +/- 1.09 (mean +/- SEM, N=8), respectively). (**B**) Stage distributions in control vehicle-treated or DHA-treated GB4, 803, 76H10^{C580Rev} and 76H10 parasite lines at *t* = 72 hours. The stage distributions were counted from Giemsa stained thin blood smears. (**C**) Timeline of intraerythrocytic delay. Bell curves represent the age distributions of control vehicle-treated or DHA-treated K13 C580 (GB4, 76H10^{C580Rev}) or C580Y (803, 76H10) parasite lines.

The dotted lines at t = 50 and at t = 72 hours indicate the collection timepoints for FACS and RSA determinations, respectively.

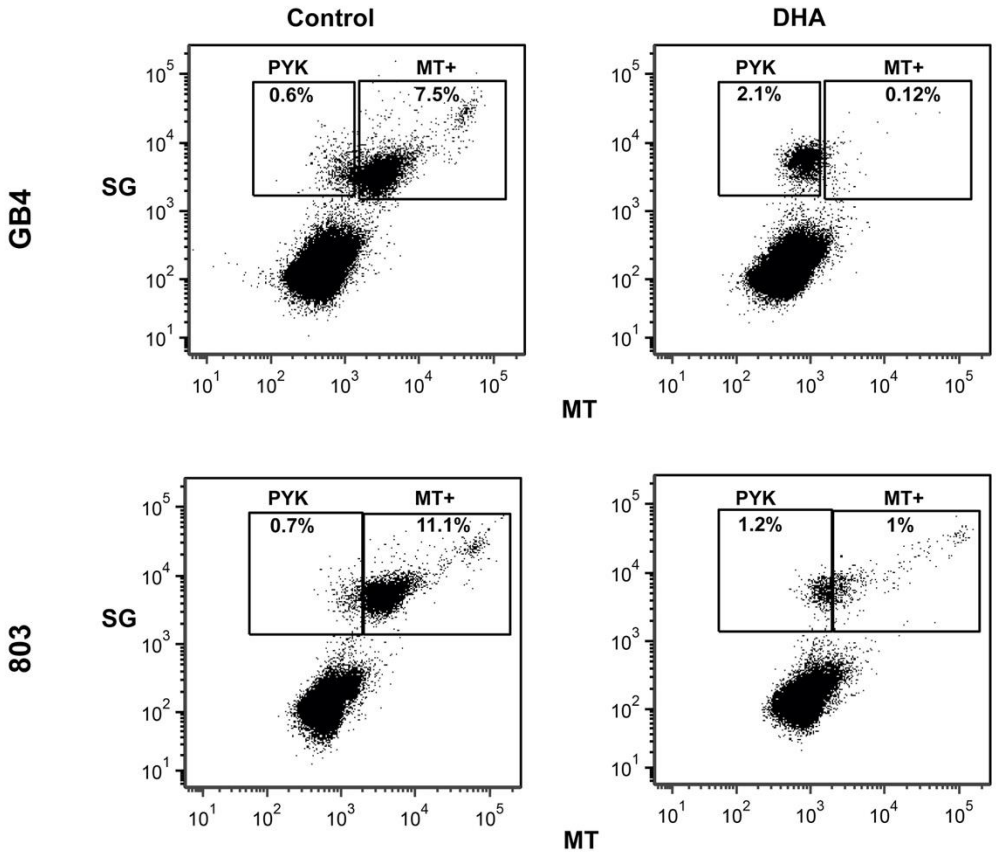

Figure 2. Representative dot plots with gating strategy for AiryScan microscopy analysis of control or DHA-treated GB4 and 803 parasites at *t* = 50 hours. The experimental procedure is shown in Figure 2 – Figure Supplement 1. In each experiment, the SG positive parasites were separated into two populations based on MT fluorescence intensity. The DHA treatments killed most parasites, as demonstrated by larger populations in the pyknotic gate (PYK). Parasites from the MT+ gate were used for ASM. SG = SYBR Green I, MT = MitoTracker Deep Red FM

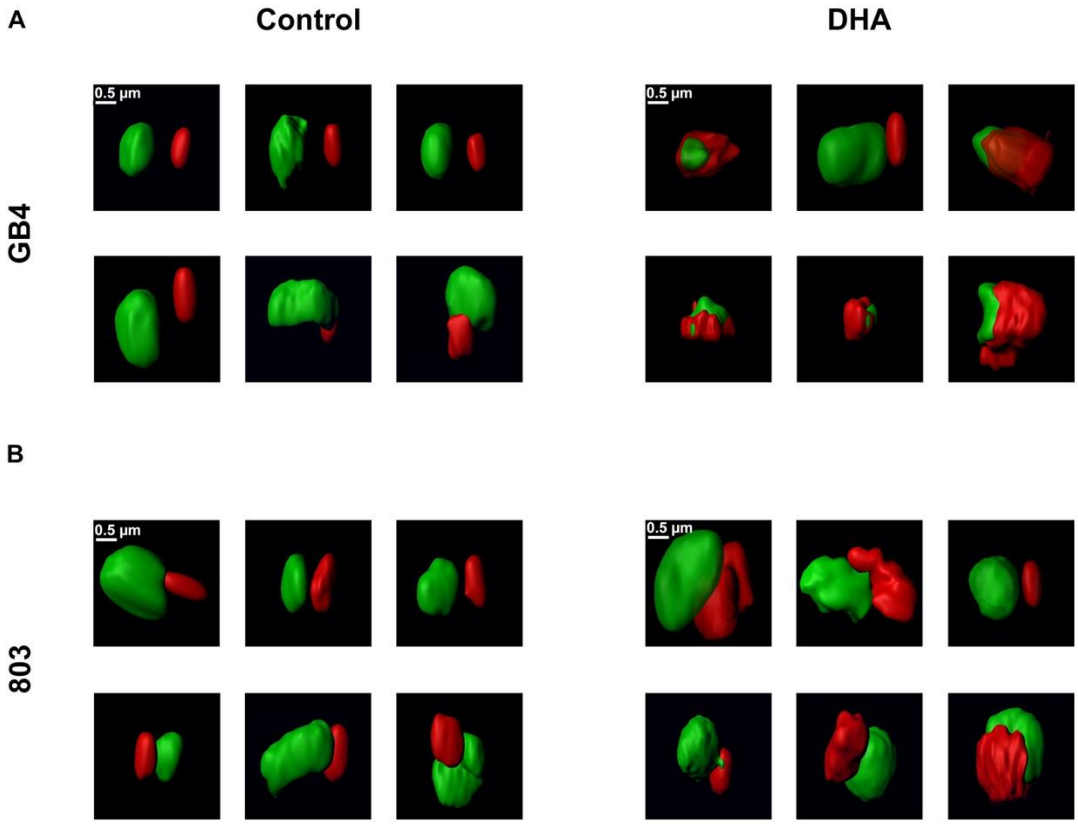

Figure 3. Airyscan microscopy images of control or DHA-treated GB4 and 803 parasites at *t* = 50 hours. Individual panels show processed ASM images of the mitochondrial (red) and nuclear (green) fluorescences from six representative parasites in each treatment group separated by FACS. (**A**) GB4 parasites from control 0.1% DMSO (vehicle) treated samples presented smooth, oblate mitochondrial and nuclear volumes. Images in the control group are consistent with young ring-stage parasites in the culture at *t* = 50 hours. DHA-treated parasites show the distinctly different morphologies of persisters, with rumpled and corrugated mitochondrial volumes that are in close approximation to the nuclei. (**B**) Images of the control 803 parasites at t = 50 hours also have the smooth, oblate appearance of mitochondria separated from the nucleus, as expected of actively replicating young parasite ring forms. Images of DHA-treated 803 parasites, in comparison to those of the treated GB4 population, are consistent with a more mixed population of cells, many with the rumpled, corrugated mitochondria closely apposed to nuclei and others with the smooth, oblate mitochondria separate from the nuclei.

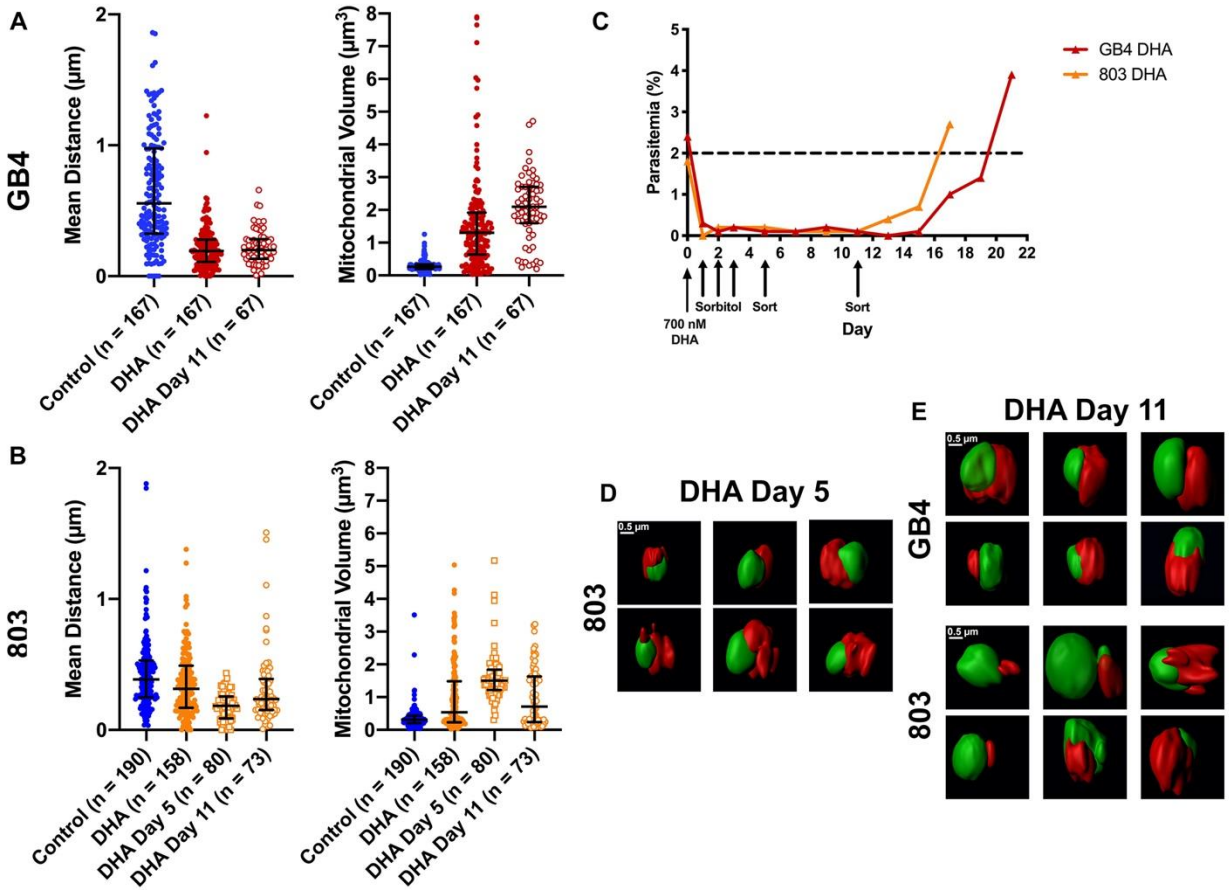

Figure 4. Quantifications of mito-nuclear distances and mitochondrial volumes of GB4 and 803 parasites at *t* = 50 hours, day 5 and day 11 post DHA treatment. Medians and interquartile ranges (IQR) are indicated over the distributions of mito-nuclear distances and mitochondrial volumes. (**A**) Scatterplots of the quantifications for each group of GB4 parasites exposed to 0.1% DMSO (control) or 700 nM DHA. (**B**) Scatterplots of the quantifications for each group of 803 parasites exposed to 0.1% DMSO (control) or 700 nM DHA. Datasets labeled control and DHA were obtained from samples *t* = 50 hours according to the schematic outline in Figure 1 – Figure Supplement 1. (**C**) Datasets on day 5 and day 11 were collected from the populations of GB4 and 803 parasites after DHA exposure and three daily sorbitol selections. GB4 parasites recrudesced to above 2% parasitemia by day 20 while 803 parasites recrudesced on day 16. In the mito-nuclear distance scatterplots, five outliers are beyond the bounds of the y-axis in the GB4 Control (2.8 µm, 2.5 µm, 2.2 µm, 2.7 µm, and 6.8 µm), one outlier in the 803 Control (3.7 µm), and three outliers in the 803 DHA results (2.6 µm, 2.0 µm, 5.5 µm). (**D**) Representative ASM images of DHA-treated 803 parasites on day 5 post treatment. Shown are six examples of persisters with rumpled, corrugated mitochondria in close approximation to the nuclei. (**E**) Surface images of DHA-treated GB4 and 803 parasites at day 11. Six representative parasites from each line are shown. Persister morphologies were evident in each parasite line, with the mitochondria in close approximation to the

nuclei. In the DHA-treated GB4 sample, large mitochondria enwrapping the nuclei were observed, similar to the persister morphology shown in Figure 3. In the DHA-treated 803 sample, persister morphology was apparent as well, but parasites with smooth oblate mitochondria that did not enwrap nuclei were frequently observed also, indicating an awakening from dormancy.

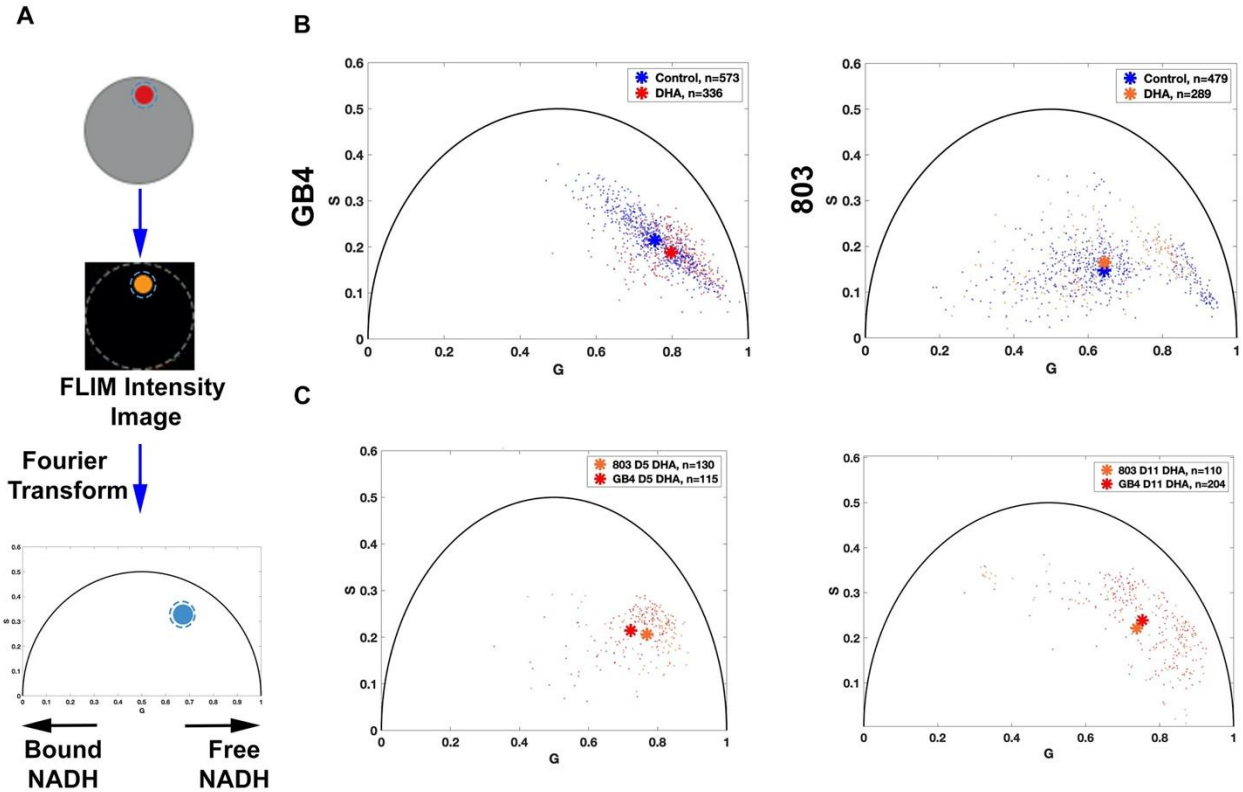

Figure 5. Metabolic phenotyping of untreated control *vs.* DHA-treated GB4 and 803 parasites. (**A**) Schematic flow of FLIM-phasor data collection and analysis. MT+ parasites were sorted and seeded into a 10 µm x 10 µm polydimethylsiloxane (PDMS) stencil microwell covered with 0.01% poly-lysine. The region of interest (ROI) in a parasite is established by the boundary of MT fluorescence. This ROI mask is then applied to the lifetime datafile represented by its FLIM intensity image. Next, Fourier transformation of the FLIM data is performed on the data from each pixel and the frequency domain results are averaged to represent a data point on the 2D phasor plot. Each position has coordinates G (from 0 to 1) and S (from 0 to 0.5); single exponential decays fall upon the semicircle whereas complex multiexponential decays, such as occur with fluorescent lifetimes of metabolic coenzymes, fall within the semicircle. A shift to the right indicates increased free NADH whereas a to the left indicates increased enzyme bound NADH. (**B**) Autofluorescence FLIM-phasor graphs from the GB4 and 803 parasite populations at t = 50 hours. The phasor distribution of untreated control GB4 parasites has a mean coordinate of (0.7542, 0.2150) whereas the distribution of DHA-treated parasites has a mean coordinate of (0.7971, 0.1879) ($p < 0.0001$, Pillai trace). This shift after DHA treatment is toward increased free NADH, consistent with the quiescent metabolic state of persisters. The distribution of untreated 803 parasites at t = 50 hours (right) has a mean coordinate of (0.6341, 0.1400) and the phasor distribution of DHA-treated parasites has a mean coordinate of (0.6270, 0.1570). The distribution of DHA-treated 803 parasites is slightly shifted upward relative to control ($p < 0.05$, Pillai trace), but not to the left or right, consistent with the presence of actively replicating 803 parasites that survived ring-stage exposure to DHA. (**C**) Autofluorescence FLIM-phasor

graphs for DHA-treated GB4 and 803 on day 5 and day 11. In the phasor distributions from day 5 (left), DHA-exposed GB4 and 803 parasites have mean coordinates of (0.72, 0.21) and (0.77, 0.21), respectively. Consistent with depletion of the many actively replicating parasites from the 803 population by three daily sorbitol treatments, the 803 phasor distribution is shifted right with quiescence and increased levels of free NADH in persisters. The varied genetic backgrounds and baseline metabolic states of African GB4 and Southeast Asian 803 parasites help to explain different positions of the 803 and GB4 coordinates ($p < 0.0001$, Pillai trace).

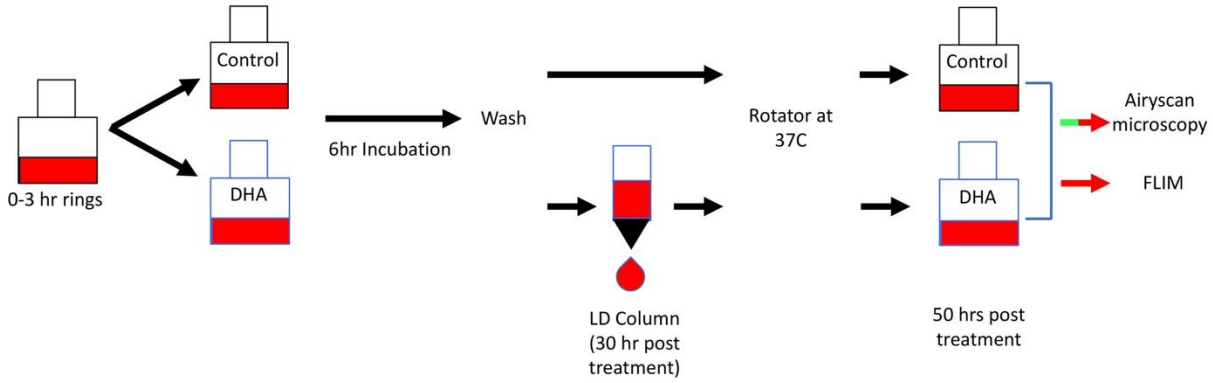

Figure 2 – Figure Supplement 1. Schematic of GB4 and 803 parasite preparations for Airyscan and FLIM-phasor analysis. GB4 or 803 parasites were synchronized through two sorbitol treatments, 46 hours apart, to obtain 0 – 3 hour rings. At the start of the experiment (*t* = 0 hours), the GB4 or 803 populations of 0 – 3 hour rings were treated at approximately 2% parasitemia with either 700 nM DHA or control 0.1% DMSO (vehicle) for 6 hours, washed and returned to culture. At *t* = 30 hours, the DHA-treated cultures were passed through a depletion column to remove mature-stage parasites that continued to actively grow after DHA treatment. Both the control and DHA-treated cultures were placed on a shaking incubator overnight to facilitate invasion of the control culture and to maintain the experimental conditions in each flask. At *t* = 50 hours, 1mL of each culture were stained with either SG plus MT for AiryScan microscopy or MT only for FLIM-phasor autofluorescence analysis.

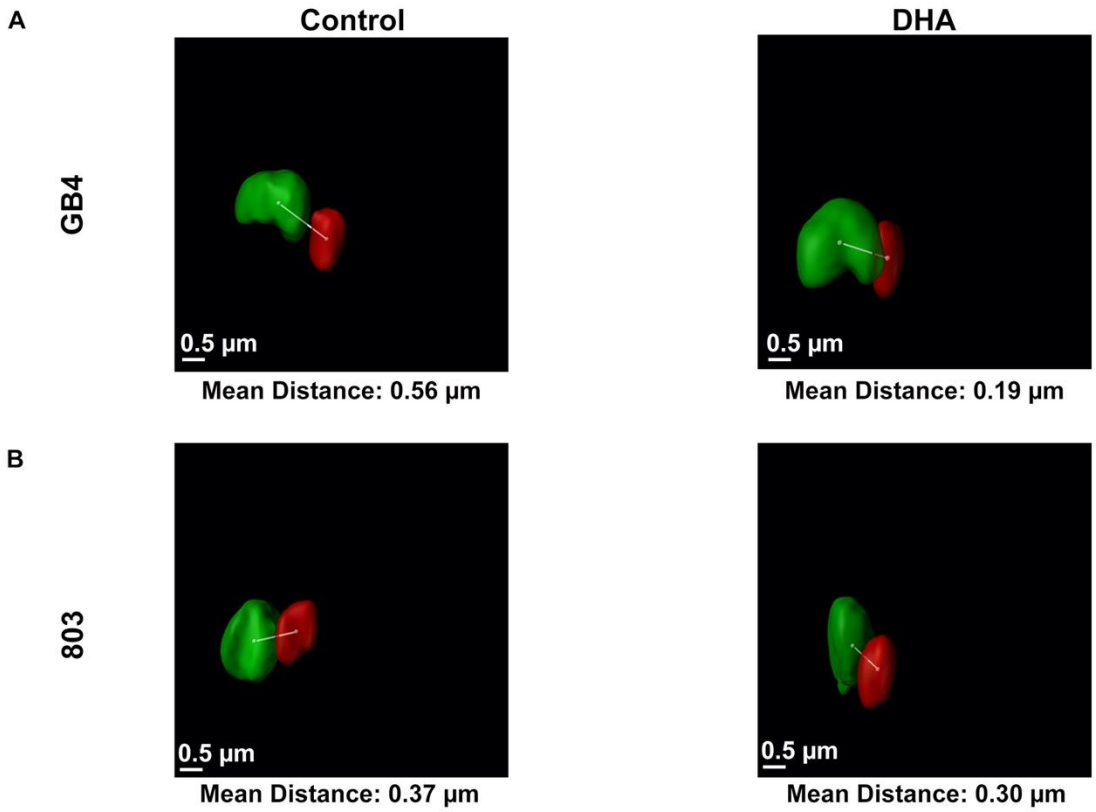

Figure 3 – Figure Supplement 1. Example ASM images showing distance between centroids in control or DHA-exposed GB4 and 803 parasites at *t* = 50 hours. The center of image mass was marked in Imaris using surfaces formed from SYBR Green I and MitoTracker Deep Red FM fluorescence regions. (**A**) GB4 parasites were exposed to control vehicle 0.1% DMSO (left panel) or 700 nM DHA (right panel). In GB4 parasites after DHA treatment, the distance between the green and red fluorescence regions was substantially reduced in the DHA-treated parasites. (**B**) In 803 parasites, similar distances were observed between the control (left panel) or DHA-treated (right panel) parasites. Mean distances were calculated between each voxel (volumetric pixel, a discrete subset of the volume with a specific 3D coordinate) and averaged for each parasite.

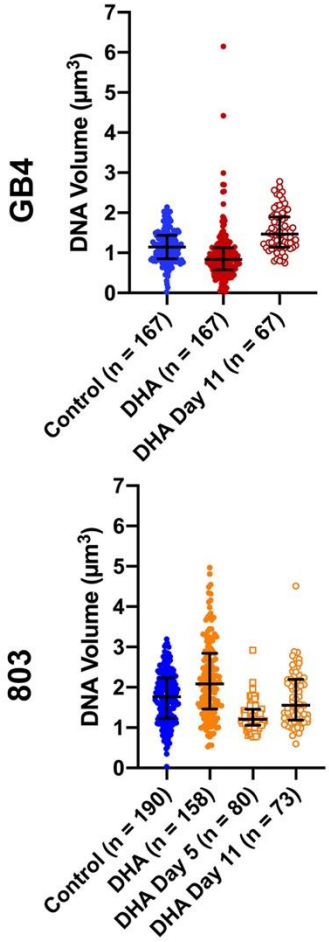

Figure 4 – Figure Supplement 1. DNA volumes of control or DHA-treated GB4 and 803 parasites at *t* = 50 hours, and of the DHA-treated parasites at days 5 and 11 in the recrudescence studies.

Supplementary File 1. Isolation of three stages of P. falciparum-infected red blood cells. Representative dot plots are shown for outgrowth experiments of control or DHA-treated GB4 and 803 parasites at *t* = 50 hours. Control or DHA-treated GB4 and 803 parasites were stained with SYBR Green (SG) and MitoTracker Deep Red (MT) and sorted using the BD FACS Aria Fusion. Labels identify dimly MT-fluorescent pyknotic cells (SG/MT^{D}), a ring-enriched population of intermediate fluorescence (SG/MT^{I}), and brightly fluorescent late stages (SG/MT^{B}).

Supplementary File 2. Results of outgrowth experiments from the fluorescent GB4 and 803 parasites isolated by FACS and collected in 1xHBSS/2% FBS. Cells were pelleted at 2500 rpm for 5 minutes and returned to culture (200 µl volume, 5% HCT) a 96 well plate. Thin and thick Giemsa stained blood smears were monitored microscopically for parasite population growth. Rows in green indicate growth; the rightmost column lists the days to 0.5% parasitemia in culture.

Supplementary File 3. Statistic results from ASM and autofluorescence FLIM-phasor analysis. Significance testing of the ASM data was by unpaired t-test calculations. In the results from autofluorescence FLIM-phasor data, mean phasor distribution coordinates were assessed for significant differences by Pillai's trace calculations between the treatment groups.